Automatized Patient-Specific Methodology for Numerical Determination of Biomechanical Corneal Response

M. Á. Ariza-Gracia [1] J. Zurita,[6] D. P. Piñero,[4,5] B. Calvo,[1,2] and J. F. Rodríguez-Matas[1,3]

[1]Applied Mechanics and Bioengineering (AMB), Aragón Institute of Engineering Research (I3A), University of Zaragoza, Zaragoza, Spain; [2]Bioengineering, Biomaterials and Nanomedicine Online, Biomedical Research Center (CIBBER-BBN), Madrid, Spain; [3]LaBS, Department of Chemistry, Materials and Chemical Engineering 'Giulio Natta', Politecnico di Milano, Milano, Italy; [4]Ophthalmology Department (OFTALMAR), Medimar International Hospital, Alicante, Spain; [5]Optics, Pharmacologist and Anatomy Department, University of Alicante, Alicante, Spain; and [6]Department of Mechanical Engineering, Energetics and Materials, Public University of Navarra, Pamplona, Spain

Associate Editor Eiji Tanaka oversaw the review of this article.

Abstract—This work presents a novel methodology for building a three-dimensional patient-specific eyeball model suitable for performing a fully automatic finite element (FE) analysis of the corneal biomechanics. The reconstruction algorithm fits and smooths the patient's corneal surfaces obtained in clinic with corneal topographers and creates an FE mesh for the simulation. The patient's corneal elevation and pachymetry data is kept where available, to account for all corneal geometric features (central corneal thickness–CCT and curvature). Subsequently, an iterative free-stress algorithm including a fiber's pull-back is applied to incorporate the pre-stress field to the model. A convergence analysis of the mesh and a sensitivity analysis of the parameters involved in the numerical response is also addressed to determine the most influential features of the FE model. As a final step, the methodology is applied on the simulation of a general non-commercial non-contact tonometry diagnostic test over a large set of 130 patients—53 healthy, 63 keratoconic (KTC) and 14 post-LASIK surgery eyes. Results show the influence of the CCT, intraocular pressure (IOP) and fibers (87%) on the numerical corneal displacement (U_{Num}), the good agreement of the U_{Num} with clinical results, and the importance of considering the corneal pre-stress in the FE analysis. The potential and flexibility of the methodology can help improve understanding of the eye biomechanics, to help to plan surgeries, or to interpret the results of new diagnosis tools (i.e., non-contact tonometers).

Keywords—FEM corneal model, Patient-specific, Sensitivity analysis, Non-contact tonometry.

Address correspondence to M. Á. Ariza-Gracia, Applied Mechanics and Bioengineering (AMB), Aragón Institute of Engineering Research (I3A), University of Zaragoza, Zaragoza, Spain. Electronic mail: mariza@unizar.es

INTRODUCTION

The corneal shape is the result of the equilibrium between its mechanical stiffness (related to the corneal geometry and the intrinsic stiffness of the corneal tissue), intraocular pressure (IOP) and the external forces acting upon it such as an external pressure. An imbalance between these parameters, e.g. an increment of IOP (glaucoma), a decrement of the corneal thickness induced by refractive surgery or by a corneal material weakening due to a disruption of collagen fibers (keratoconus), can produce ocular pathologies (ectasias) which seriously affect patient's sight. Consequently, it is important to understand how ocular factors such as IOP, geometry and corneal material are related to pathologies in order to improve treatments. The first step in this direction consists of the correct measurement of the IOP and corneal topography. To date, the IOP is measured by either contact tonometers (e.g. Goldmann Applanation Tonometry)[22,30] or non-contact tonometers, e.g. CorVis ST (Oculus Optikgeräte GmbH),[14] whereas the corneal topography is obtained with corneal topographers, e.g. Pentacam (Oculus Optikgeräte GmbH) and Sirius (Schwind eye-tech-solutions GmbH & Co.KG),[3] which have reached a high level of sophistication and accuracy.

The availability of high resolution topographical data and the patient's IOP have made possible to reconstruct a patient's specific geometric model of the cornea, which makes it possible to study specific treatments and pathologies. In this regard, some patient-specific corneal models have already been reported in the literature.[29,32] However, the pipeline

described in these studies cannot be automated in a straightforward manner as to permit personalized analysis on large populations. Another limitation is that these methodologies rely on an approximation of the topographical data when building the corneal model. Studer et al.[32] used Zernike polynomials to generate anterior and posterior corneal surfaces by approximating the available topographical data instead of directly incorporating the corneal thickness and curvature provided by the topographer. In addition, these numerical models did not provide an appropriate mesh convergence analysis so as to check the accuracy of the results.

An accurate numerical model of the eye is based on the identification of an adequate strain energy function from which the stress–strain relationship of the cornea is obtained. To achieve it, an understanding of the underlying structure of the tissue is needed. The cornea is composed of four different layers: epithelium, bowman's membrane, stroma and endothelium. The stroma represents the major part of the cornea and is formed by different orthogonally crossed lamellae, which are made of collagen fibers. The corneal collagen is organized in two preferential directions:[18,19,21] (i) Nasal–Temporal direction, and (ii) Superior–Inferior direction. On the contrary, limbus collagen fibers are disposed circumferentially.[23–25] These characteristics provide the cornea with a highly anisotropic behavior in addition to a nearly incompressible response.[4] Even though the cornea shows an intrinsic viscoelastic behavior, for most applications it may be described as a nonlinear anisotropic hyperelastic solid.[18,23,24] Additionally to these considerations on the mechanical response, it should be noticed that topographers measure the deformed geometry of the cornea under the action of the IOP but the stress and strain fields still remain unknown. Therefore, it is necessary to obtain a free-stress configuration of the eyeball that faithfully represents the load free configuration of the cornea. Elsheikh et al.[8] and Roy et al.[29] proposed an iterative geometric algorithm by varying IOP in order to obtain the reference eyeball geometry, whereas Studer et al.[32] and Lanchares et al.[18] proposed a pre-stressing algorithm based on the deformation gradient. However, these algorithms did not incorporate a consistent mapping of the direction of collagen fibers onto the identified load free configuration (zero-pressure configuration). Riveros et al.[27] have proposed a general pullback algorithm for nonlinear anisotropic materials in which the direction of collagen fibers are consistently mapped onto the identified zero-pressure configuration, which has already been applied to vascular geometries.

The aim of this work is to develop a robust methodology to incorporate a patient's specific corneal topology into a finite element (FE) model of the eyeball, accounting for the free-stress configuration of the eyeball, and taking into account the hyperelastic anisotropic material response of the corneal tissue. Furthermore, the proposed pipeline is demonstrated on a set of 130 patients (53 healthy, 63 keratoconic and 14 post-LASIK eyes) following a general non-commercial non-contact tonometry protocol. Despite the use of an air-puff diagnostic test to validate the methodology, other types of test (i.e., inflation test or different surgical interventions) could be easily implemented and simulated. Finally, several results are addressed such as: the search for the most influential parameters on the numerical model by means of a sensitivity analysis based on the Design of Experiments theory[20] (2^k full factorial and ANOVA analysis), the effect of the zero-pressure configuration on the model behavior and, to conclude, the comparison of the numerical results (displacements) with previous data reported in the literature from simulation[16] and clinical studies.[12,28]

MATERIAL AND METHODS

For a better comprehension and follow-up, the section is organized as the proposed pipeline for the patient-specific corneal modeling (see in Fig. 1), from the topographical imaging acquisition to the desired FE simulation. The framework comprises five main steps namely: (i) Step-1: Topographic Data Acquisition, (ii) Step-2: Corneal Surface Reconstruction, (iii) Step-3: Numerical Model of the Cornea, (iv) Step-4: Zero-Pressure Algorithm, and (v) Step-5: Computer Simulation and Sensitivity Analysis.

Step-1: Topographic Data Acquisition

Clinical data from patients were collected prospectively, i.e., an ongoing measuring process without posterior revision of the patient's medical history, at the Department of Ophthalmology (OFTALMAR) of the Vithas Medimar International Hospital (Alicante, Spain). A comprehensive ophthalmologic examination was performed in all cases including: LogMAR uncorrected distance visual acuity (UDVA), LogMAR corrected distance visual acuity (CDVA), manifest refraction (sphere and cylinder), slit-lamp biomicroscopy, Goldmann tonometry, fundus evaluation, and corneal and anterior segment analysis by means of a Scheimpflug photography-based topography system, the Pentacam system version 1.14r01 (Oculus Optikgeräte GmbH, Germany). The patients wearing contact lenses for the correction of the refractive error were instructed in all cases to discontinue the use of contact lenses for at least 2 weeks before each exami-
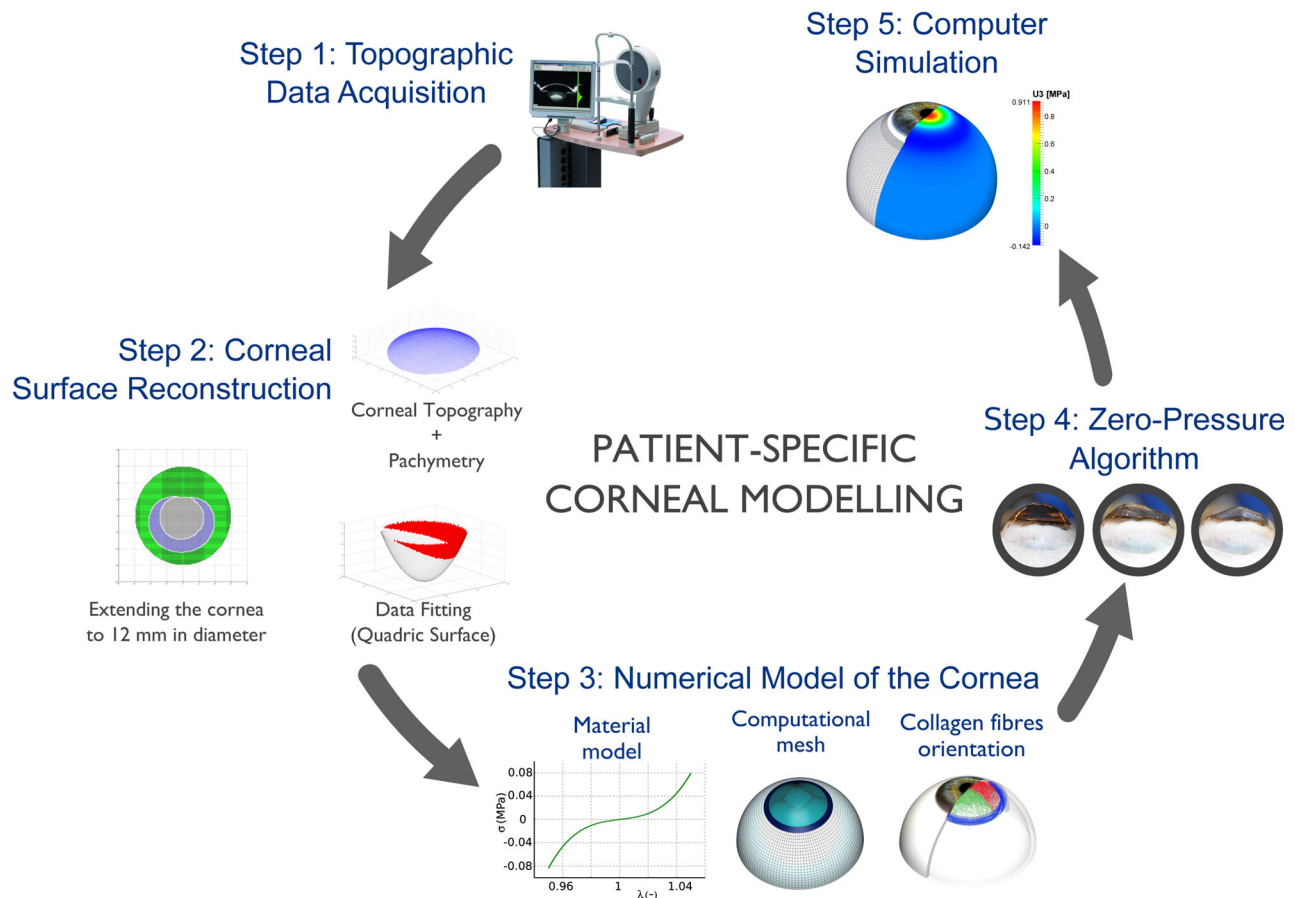
FIGURE 1. General pipeline of the proposed framework for patient-specific corneal modeling from the clinical image (image-based geometry) to the computer simulation (general non-contact tonometry). It is composed of five main steps: (1) Topographic Data Acquisition; (2) Corneal Surface Reconstruction; (3) Numerical Model of the Cornea; (4) Zero-Pressure Algorithm and (5) Computer Simulation (general non-commercial non-contact tonometry).

nation for soft contact lenses and at least 4 weeks before each examination for rigid gas permeable contact lenses. All volunteers were adequately informed and signed a consent form before the inclusion in the study. The study adhered to the tenets of the Declaration of Helsinki and was approved by the ethics committee of the University of Alicante (Alicante, Spain). Inclusion criteria were healthy eyes, eyes with the diagnosis of keratoconus according to the Rabinowitz criteria,[26] or eyes that had undergone previous laser in situ keratomileusis (post-LASIK) for the correction of myopia (range −0.50 to −8.00 D). Exclusion criteria were patients with active ocular diseases or patients with other types of previous ocular surgeries.

The Oculus Pentacam is a noninvasive system for measuring and characterizing the anterior segment using a rotating Scheimpflug camera which generates Scheimpflug images in three dimensions, with a dot matrix fine-meshed in the center due to the rotation. The full process takes a maximum of 2 s to generate a complete image of the anterior eye segment. A second camera detects any movement artefact (e.g. eye movement) so as to correct feasible measuring setbacks. The Pentacam calculates a 3-dimensional topographical model of the anterior eye segment using as many as 25,000 true elevation points. The images taken during the examination are digitalized in the main unit and transferred to a computer and analyzed in detail.

Gathered Pentacam corneal topographies (data from other topographers such as Sirius can also be handled) are represented as point cloud surfaces in the form of two 141×141 matrices. The first matrix contains the coordinates (x, y, z) of the anterior corneal surface, whereas the second matrix represents the available pachymetry (corneal thickness) data at each (x, y) point. Since pachymetry data are sometimes not available at all points in the anterior surface point cloud, the number of non-zero elements in the pachymetry matrix determines the total number of available

data points for surface reconstruction. The posterior surface is the result of a point-to-point subtraction between the anterior surface and the pachymetry data.

Step-2: Corneal Surface Reconstruction

A reliable patient-specific FE model of the cornea must incorporate patient's topographical data as much as possible. In this regard, the proposed framework makes use of actual patient's data where available, minimizing the amount of extrapolated data required to build a full three-dimensional FE model amenable for numerical simulations. Current topographers provide topographical data limited to a corneal area between 8 and 9 mm in diameter due to patient misalignment, blinking or eyelid aperture (see Fig. 2a). However, a corneal diameter of 12 mm (average human size) is needed to build a 3D FE model.[29,32]

In order to overcome this limitation, a surface continuation algorithm is proposed. Data extrapolation is performed by means of a quadric surface given in matrix notation as

$$\mathbf{X}^T \mathbf{A} \mathbf{X} + 2\mathbf{B}^T \mathbf{X} + c = 0, \tag{1}$$

where $\mathbf{A}$ is a 3×3 constant matrix, $\mathbf{B}$ is a 3×1 constant vector, and c is an scalar, which define the parameters of the surface. Equation 1 is fitted to the topographical data by means of a nonlinear regression analysis.

To extend the corneal surface, the quadric surface (Eq. 1) should properly approximate the periphery of the patient's topographical data (blue area in Fig. 2a). For this reason and before fitting the Eq. (1), the central corneal part is removed using a level set algorithm based on the relative elevation of each corneal point with respect to the apex. In brief, starting at a relative elevation of 1, i.e., the apex, and reducing in
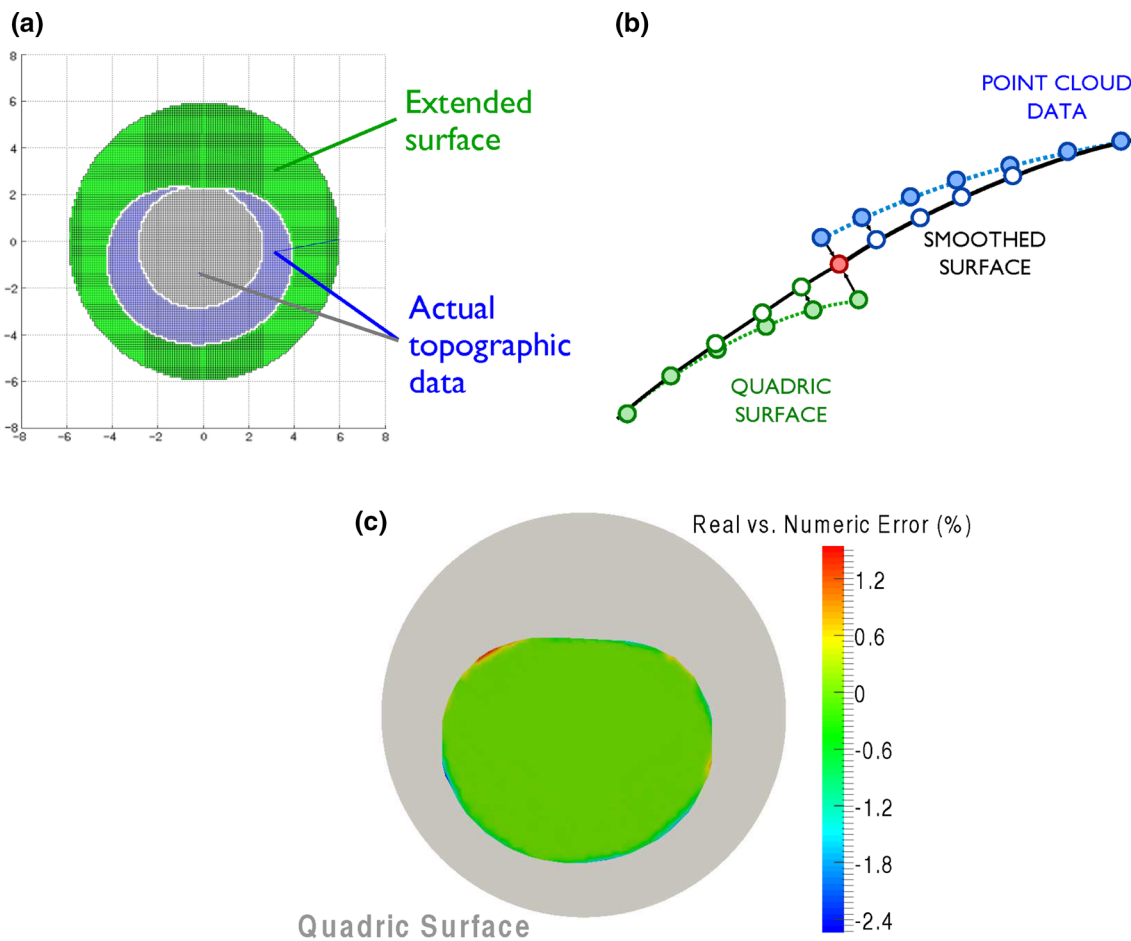

FIGURE 2. Corneal surface reconstruction (Extreme post-LASIK eye used as example). (a) Projection of the 12 mm diameter corneal surface in the optical axis plane. Grey and blue shaded surfaces correspond to the corneal surface measured by the topographer (image-based geometry). Green area corresponds to the extended surface required in order to achieve a 12 mm diameter (approximating surface); (b) Surface smoothing at the joint between the extended surface and the patient's corneal surface; (c) Contour map of the error between the point cloud data prior and after smoothing (less than a 5% at the corneal periphery).

steps of 0.005, subsequent level sets are identified (see gray area in Fig. 2a). When the size of the level set, i.e., radius of the circumscribe circle, changes by less than a 15% between two consecutive increments, the algorithm stops. Corneal periphery is then obtained by subtracting the identified level set from the topographic data (blue area in Fig. 2a).

When using an analytical surface as Eq. (1) to extend the corneal surface, there will always be a jump at the joint between the approximating surface and the point cloud surface (see Fig. 2b). This discontinuity in the normal of the surface may lead to convergence problems or to non-realistic stress distributions on the cornea during the FE analysis. Hence, a smoothing algorithm based on the continuity of the normal between the quadric surface and the point cloud data is applied as shown in Fig. 2b, producing local alterations in the patient's topographic data near the border. However, these alterations are very small (less than a 3%) as outlined in the contour map of the error between the topographic point cloud data prior and after smoothing (Fig. 2c), where the depicted data corresponds to an extreme post-LASIK patient (also used for testing the performance of the corneal surface reconstruction algorithm, see Fig. 3c).

The performance of the corneal reconstruction algorithm was demonstrated on three extreme cases: (i) a healthy right cornea of a 50-year woman, with an apex pachymetry of 593 microns, a minimum pachy-metry of 586 microns, a nasal-temporal radius of 7.63 mm and a superior–inferior radius of 7.79 mm; (ii) a left cornea of a 60-year man affected by a kerato-conus (KTC), with an apex pachymetry and a minimum pachymetry of 499 microns, a nasal–temporal radius of 6.87 mm and a superior–inferior radius of 7.69 mm; and (iii) a post-LASIK refractive surgery, which is the right cornea of a 60-year woman, with an apex pachymetry of 379 microns, a minimum pachy-metry of 375 microns (a particularly extreme case due to the large reduction in pachymetry after surgery), a nasal–temporal radius of 11.69 mm and a superior–inferior radius of 11.24 mm. In all cases, topographical data was acquired using a Pentacam topographer.

The approximation error obtained with the quadric surface and a traditional sphere approximation with respect to the real surface, i.e., the subtraction error between the theoretical approximating surface and the real surface provided by the topographer, is shown in Fig. 3 for the three considered extreme ocular geometries. For the Healthy eye, the sphere fits the corneal apex better than the corneal borders (in terms of the lowest difference between the real topographic surface and the approximating surface) with an error difference ranging from 33.6 to -74.4 microns (Fig. 3a top panel), whereas the quadric surface fits the corneal periphery better than the corneal apex with an error difference ranging from 21.5 to -30.3 microns (Fig. 3a bottom panel). Considering the
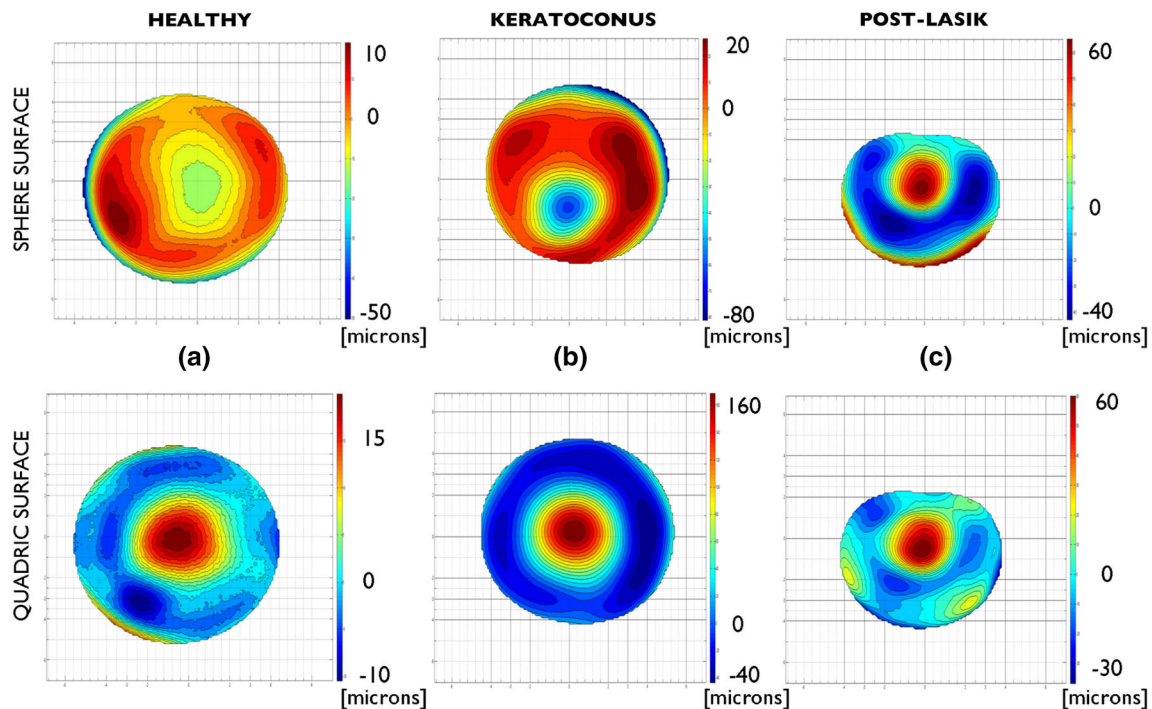

FIGURE 3. Subtraction error, i.e., difference between the image-based geometry (point cloud obtained by the topographer) and the approximating surface, measured on microns (μm), depending on surface fitting typology (top panel—sphere/bottom panel—quadric): (a) healthy eye, (b) keratoconus eye, (c) post-LASIK eye.

KTC eye, the sphere fits the corneal center (excepts at the KTC location) better than the corneal borders with an error difference ranging from 49.9 to −102.2 microns (Fig. 3b top panel), whereas the quadric fits the corneal periphery better than the corneal center, where the pathology is very underestimated, with an error difference ranging from 180.1 to −57.1 microns (Fig. 3b bottom panel). Regarding the post-LASIK eye, the sphere fits the corneal center (excepts at the location of the surgery) better than the corneal borders with an error difference ranging from 71 to −47.4 microns (Fig. 3c top panel), whereas the quadric fits the corneal periphery better than the center of the cornea with an error difference ranging from 65.2 to −36.7 microns (Fig. 3c bottom panel). These results indicate that a sphere surface fits better at the center of the cornea while a quadric surface fits better at the periphery of the cornea (always in terms of the lowest difference between the real topographic surface and the approximating surface).

Therefore, the quadric surface model is better suited to extend the cornea to 12 mm in diameter as required by the FE model. Furthermore, regarding the surface fitting, the mean and the standard deviation of the quadric surface coefficients for the entire population (53 healthy, 63 keratoconic and 14 post-LASIK surgery) have been analyzed to observe the correctness of the numerical fitting on reproducing the corneal surface there where the topographer is unable to measure (see in Table 1). The coefficients associated with the quadratic terms clearly dominate indicating that the cornea is well approximated by an oblate spheroid (Note that A is very similar to B whereas C is a smaller order of magnitude). Hence, these results are consistent with the geometry of the cornea.

Step-3: Numerical Model of the Cornea

Material Description

Since the cornea is considered an anisotropic hyperelastic material, Gasser–Holzapfel–Ogden's strain energy function (G–H–O)[9,13] is proposed to describe its constitutive behavior.

$$U = \frac{1}{D} \cdot \left(\frac{J_{el}^2 - 1}{2} - ln(J_{el}) \right) + C_{10} \cdot (\bar{I}_1 - 3)$$
$$+ \frac{k_1}{2 \cdot k_2} \cdot \sum_{\alpha=1}^{N} \{ \exp[k_2 \langle \bar{E}_\alpha \rangle^2] - 1 \} \quad (2)$$
$$\bar{E}_\alpha \overset{def}{=} \kappa \cdot (\bar{I}_1 - 3) + (1 - 3\kappa) \cdot (\bar{I}_{4(\alpha\alpha)} - 1),$$

where $\bar{I}_1$ is the first invariant of the modified right Cauchy–Green tensor $\bar{\mathbf{C}} = J_{el}^{-2/3} \mathbf{C}$, J_{el} is the elastic volume ratio, $\bar{I}_{4(\alpha\alpha)}$ is a pseudo-invariant that represents the square of the stretch along the direction of the α-th family of collagen fibers, being N the total number of families of collagen fibers (two for the human cornea). D represents the inverse of the volumetric modulus. The dispersion parameter, κ, $(0 \leq \kappa \leq \frac{1}{3})$ determines the anisotropic grade: $\kappa = 0$ implies transversely isotropy, and $\kappa = 3$ implies isotropy. In addition, Eq. (2) assumes that collagen fibers only work under traction, i.e., $\bar{E}_\alpha > 0$.

The material constants concerning the corneal and limbal constitutive model were obtained by means of nonlinear regression analysis of a typical IOP-apical rise curve:[2,35] $C_{10} = 0.05$ (MPa), $D = 0.0$ (MPa^{-1}), $k_1 = 130.9$ (MPa), $k_2 = 2490.0$ [–] and $\kappa = 0.33329$ [–]. For the computations, the same mechanical properties and dispersion parameter have been assumed for all families of fibers. Figures 4a and 4b show the stress–stretch and IOP-apical rise curves predicted with the proposed material model and also demonstrate that the numerical predicted IOP-apical rise curve is within the reported human range[2,35] (see in Fig. 4b).

The sclera has been assumed as an isotropic hyperelastic material[7] Eq. (3). The distribution of fibers within the sclera far from the optical nerve insertion do not seem to follow a preferential direction, showing a random pattern and, therefore, it is likely to present a more isotropic behavior near to its equatorial

TABLE 1. Mean and standard deviation of the quadric surface coefficients sorted by population.

| Equation Coeffs.	$A \cdot x^2 + B \cdot y^2 + C \cdot z^2 + 2D \cdot xy + 2E \cdot xz + 2F \cdot yz + 2G \cdot x + 2H \cdot y + 2I \cdot z = 1$								
	A	B	C	D	E	F	G	H	I
Population	Healthy								
Mean	−0.1275	−0.1310	−0.0771	−0.0001	−0.0001	0.0022	0.0002	−0.0066	0.9212
Std	0.0092	0.0098	0.0158	0.0012	0.0037	0.0025	0.0083	0.0038	0.0504
Population	KTC								
Mean	−0.1476	−0.1566	−0.0501	0.0003	0.0009	0.0194	−0.0016	−0.0062	0.9776
Std	0.0334	0.0351	0.0676	0.0038	0.0132	0.0179	0.0130	0.0173	0.0986
Population	Lasik								
Mean	−0.1405	−0.1457	−0.0917	0.0004	0.0016	0.0008	−0.0062	−0.0044	1.0124
Std	0.0173	0.0188	0.0326	0.0016	0.0034	0.0036	0.0096	0.0063	0.1079
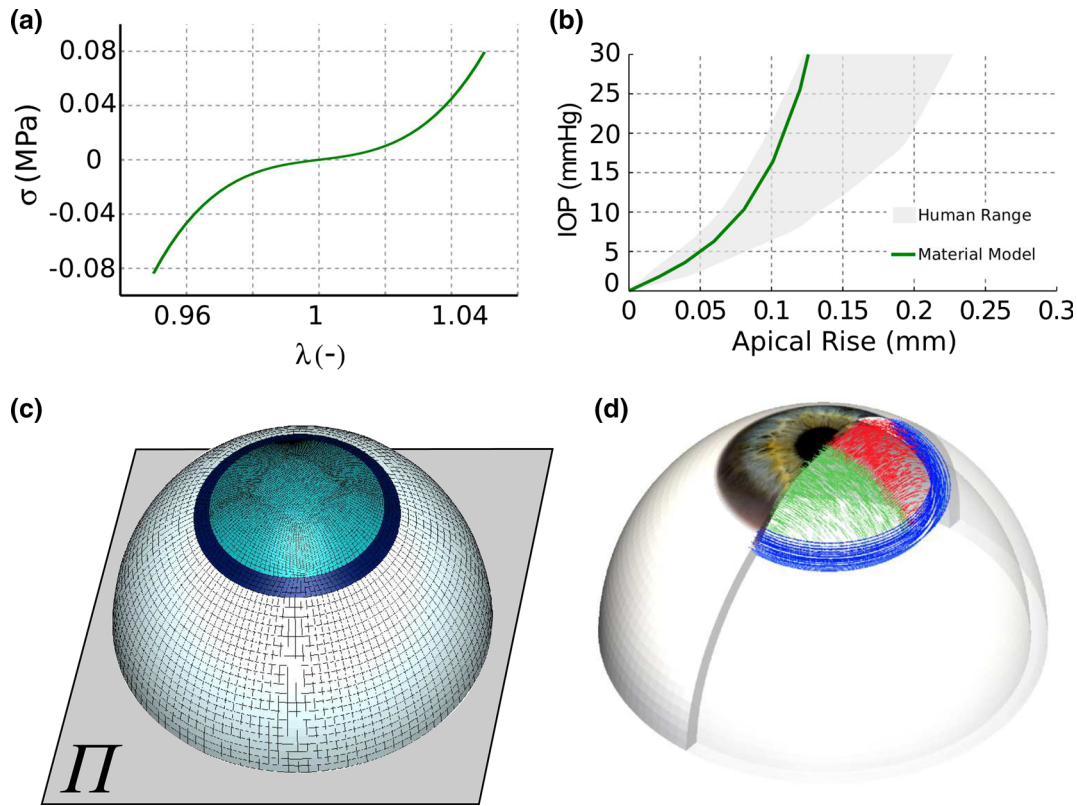
FIGURE 4. Numerical model of the eyeball. (a) Stress-stretch ($\sigma - \lambda$) curve for the corneal material model. σ is the cauchy stress of the apex and λ is the stretch; (b) IOP-apical rise curve predicted by the material model. IOP is the intraocular pressure and the apical rise is the relative displacement of the apex when IOP increase. Grey area belongs to the reported human range;[35] (c) Finite element mesh of the eye ball: Sclera (white region), Limbus (dark blue region), Cornea (light blue region); (d) Direction of collagen fibers. Two orthogonal directions for the cornea (red and green fibers), and one circumferential direction for the limbus (blue fibers).

plane than an the anisotropic behavior on the surroundings of the optical nerve.[6] In addition, the cornea plays the main role in our simulation study, since it receives the air-jet impact, whereas the sclera plays a secondary role as a more natural non-restrictive boundary condition for the cornea, much better than restraining nodal displacements or imposing theoretical boundary conditions on the corneal periphery. Furthermore, the scleral material has proved to be much stiffer than the corneal.

$$U = \sum_{i=1}^{3} \frac{1}{D_i}(J_{el} - 1)^{2 \cdot i} + \sum_{i=1}^{3} C_{i0} \cdot (\bar{I}_1 - 3)^i, \quad (3)$$

with $C_{10} = 0.81$ (MPa), $C_{20} = 56.05$ (MPa), $C_{30} = 2332.26$ (MPa), $D_i = 0.0$ (MPa^{-1}).

Finite Element Model

Once the corneal surface fitting is completed, it is introduced in the three-dimensional model of the anterior half ocular globe, which accounts for three different parts: the cornea, the limbus and the sclera. Since only the cornea can be partially measured by a topographer and neither the sclera nor the limbus can be measured with this procedure, average parts are used instead. The sclera was assumed as a 25 mm in diameter sphere with a constant thickness of 1 mm, whereas the limbus is a ring linking both, the sclera and the cornea. The geometry has been meshed using hexahedral elements by means of an in-house C program as shown in Fig. 4c, thus allowing precise control of the mesh size, as well as generating meshes with trilinear (8-nodes) or quadratic (20-nodes) hexahedral elements. Pachymetry data measured with the topographer is accurately mapped onto the three-dimensional finite element model during mesh generation. Finally, the FE model of the eyeball is completed by defining the corneal fibers over the two preferential orientations (a nasal-temporal and superior-inferior directions) and one single circumferential orientation embedded in the limbus (Fig. 4d).

Symmetry boundary conditions have been defined at the scleral equator (Π plane in Fig. 4c),[18,25] i.e., the base of the semi-sclera which does not account for the optical nerve insertion since it is not necessary for the present simulation, in such a way that the boundary
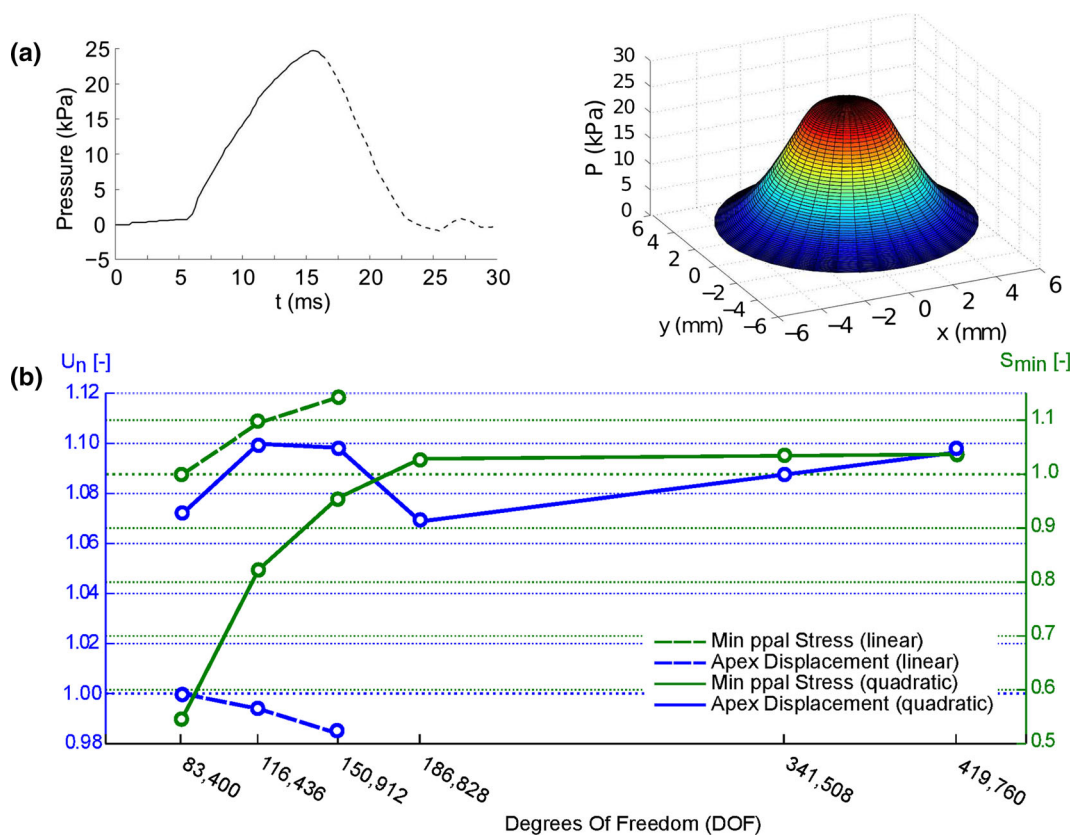
FIGURE 5. Mesh convergence analysis of the FE model. (a) Left panel: Temporal pressure profile applied on the center of the cornea to simulate a non-contact tonometry test. Solid black line represents the temporal profile used in the simulations (up to 15 ms only). Right panel: Spatial pressure profile applied on the cornea's anterior surface obtained by means of a CFD simulation; (b) Relative change in the maximum apical displacement, U_n, (blue lines) and the minimum principal stress, S_{min}, in the cornea (green line) as a function of the number of degrees of freedom (D.O.F.) in the mesh for trilinear elements (discontinuous line) and quadratic elements (continuous line). Results are normalized respect to the coarsest mesh (83,400 D.O.F.).

nodes are allowed to move on the symmetry plane Π than fixing all nodal degrees of freedom.[29,32] In addition, the inner surface of the eyeball is subject to the actual patient's IOP, which was previously measured by means of Goldmann applanation tonometry.

Computation time and accuracy are both the most important parameters when conducting an FE analysis but, unfortunately, the higher the accuracy required, the greater the computing time also required. In order to reach an optimal trade-off between both, a convergence analysis of the finite element mesh was performed based on the simulation of a general non-commercial non-contact tonometry test. Linear and quadratic elements were considered, varying the number of elements through the corneal thickness from 2 to 8 elements (4, 6, and 8 for linear elements, and 2, 3, 4, and 5 for quadratic elements), and the maximum element size from 0.3 to 0.2 mm. The maximum apical displacement and the minimum principal stress have been considered as monitor variables of the convergence analysis. Regarding the features of the FE simulation, the air-puff acting on the

anterior corneal surface was assumed as a metered collimated air pulse with a peak pressure of 25 kPa (approx. 180 mmHg), the loading phase (first 15 ms) of the entire temporal pressure profile (total duration of 30 ms) was considered (see in Fig. 5a, left panel) and, finally, the spatial distribution of the pressure over the cornea (see in Fig. 5b, right panel) was defined by performing a CFD simulation over a single healthy average model with the commercial software ANSYS (ANSYS, Inc.), in order to obtain a more realistic pressure distribution.[2] The complete FE analysis was performed using the commercial finite element software ABAQUS (Dassault Systemes Simulia Corp.).

Figure 5b shows the relative change in the maximum apical displacement and minimum principal stress as a function of the mesh size (degrees of freedom—D.O.F.). Results in Fig. 5b have been normalized with respect to those obtained for the coarsest mesh. In general, trilinear elements show a much slower rate of convergence as compared to quadratic elements, besides predicting slightly shorter apical displacements and larger stresses. In this regard, the maximum apical displacement and the

minimum principal stress change by less than 0.05 and 5%, respectively when using a mesh with more than 186,000 D.O.F. (62,000 nodes) and quadratic elements. Another remarkable aspect of the convergence analysis concerns the computation time, since a model with 186,000 D.O.F. composed of trilinear hexahedra takes about three times more computing time than the equivalent model meshed with quadratic elements (results not shown).

Based on the convergence analysis, the FE model is generated with quadratic hexahedra and 5 elements through the thickness (11 nodes), resulting in an eyeball with 62,276 nodes (186,828 degrees of freedom) and 13,425 quadratic elements.

Step-4: Zero-Pressure Algorithm

When an eye is measured by a topographer, the identified geometry belongs to a deformed configuration due to the effect of the IOP (hereafter referred to as the image-based geometry) but the corneal pre-stress is neglected. Hence, an accurate stress analysis of the cornea starts by identifying the initial state of stresses due to the physiological IOP present on the image-based geometry, or equivalently, the actual geometry associated with the absence of IOP (hereafter referred to as the zero-pressure geometry) as shown in Fig. 6a. Consequently, an iterative algorithm is used to find the zero-pressure configuration of the eye[27] (see algorithm in Fig. 6b) that keeps the mesh connectivity unchanged

(a) Deformed Corneal Geometry   Zero Pressure Corneal Geometry

$\mathbf{X}_{REF}$ $\mathbf{X}_K$

(b)

GIVEN
$\boldsymbol{X}_{REF}$, fibres direction $\boldsymbol{M}$ and $\boldsymbol{N}$, itemax, TOL

INITIALIZE
k=0, $\boldsymbol{X}_k = \boldsymbol{X}_{REF}$, $\boldsymbol{M}_k = \boldsymbol{M}$, $\boldsymbol{N}_k = \boldsymbol{N}$

REPEAT

   i) FE Analysis: internal pressure $(IOP*)$
     $\boldsymbol{X}_k^d \rightarrow \mathrm{ABAQUS}(\boldsymbol{X}_k, \boldsymbol{M}_k, \boldsymbol{N}_k)$
     $\mathbf{E}_k = \boldsymbol{X}_k^d - \boldsymbol{X}_{REF}$
     $e_k = \|\boldsymbol{X}_k^d - \boldsymbol{X}_{REF}\|_\infty$

  ii) Update zero-pressure geometry
     $\boldsymbol{X}_{k+1} = \boldsymbol{X}_k - \mathbf{E}_k$

 iii) Fibre pull—back (Cornea & Limbus)
     Deformation Gradient $\boldsymbol{F}^{k+1} = \frac{\partial \boldsymbol{X}_{REF}}{\partial \boldsymbol{X}_{k+1}}$
     $\boldsymbol{M}_{k+1} = (\boldsymbol{F}^{k+1})^{-1}\boldsymbol{M}$
     $\boldsymbol{N}_{k+1} = (\boldsymbol{F}^{k+1})^{-1}\boldsymbol{N}$

 iv) k=k+1

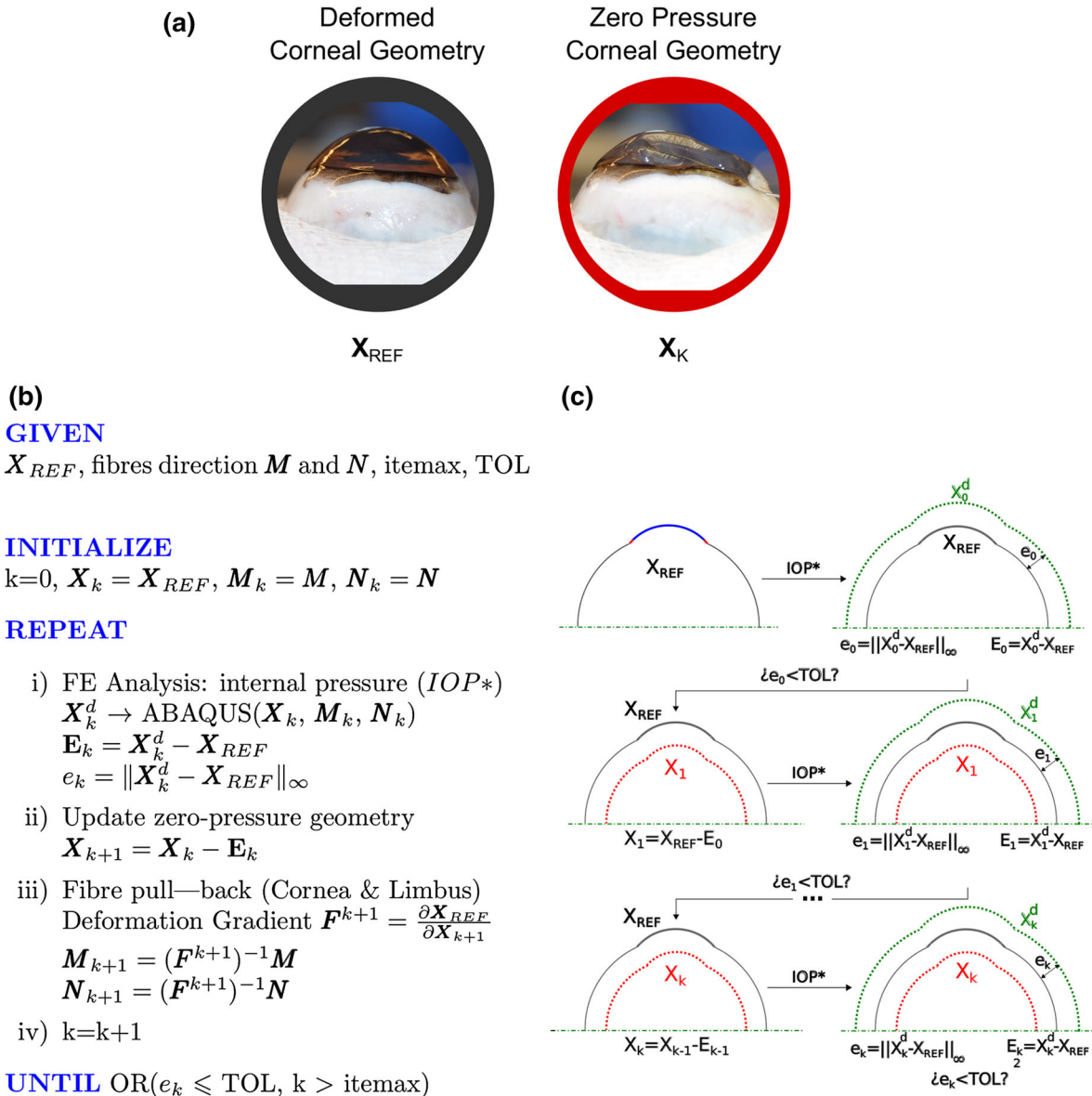**UNTIL** $\mathrm{OR}(e_k \leqslant \mathrm{TOL}, k > \mathrm{itemax})$

(c)

FIGURE 6. (a) Influence of the IOP in the corneal shape (dog's cornea); (b) Zero-pressure algorithm accounting for the pull-back algorithm with a consistent mapping of the fibers onto the current unloaded state; (c) Iterative scheme of the algorithm.

and iteratively updates the nodal coordinates. Moreover, the local directions of anisotropy (orientation of collagen fibers) are also consistently pulled-back to the current zero-pressure configuration.

In Fig. 6, X_{REF} stands for the patient's geometry reconstructed from the topographer's data, where X represents a $N_n \times 3$ matrix that stores the nodal coordinates of the finite element eyeball, with N_n the number of nodes in the FE mesh, i.e., 62,276 nodes; X_k is the zero-pressure configuration identified at iteration k; and X_k^d is the deformed configuration obtained when inflating the zero-pressure configuration X_k at the IOP pressure. The iterative algorithm updates the zero-pressure geometry, X_k, until the infinite norm of the nodal error between X_{REF} and X_k^d is less than a tolerance, TOL. The algorithm is described as follows:

Initialization: fiber directions, M and N, are defined in the reconstructed corneal geometry (image-based geometry). Tolerance TOL and maximum number of iterations $itemax$ are defined, and counter k is initialized.

Step i: At the $(k+1)$-th iteration an FE stress analysis is performed considering the zero-pressure configuration computed in the k-th iteration, X_k, as the reference configuration yielding to the deformed configuration at k-th iteration, X_k^d. Boundary conditions and IOP (IOP*) are applied as described in the previous section.

Step ii: The $(k+1)$-th zero-pressure geometry is computed as $X_{k+1} := X_k - (X_k^d - X_{REF})$.

Step iii: The fibers are consistently mapped onto the k-th zero-pressure geometry as $M_{k+1} = (F^{k+1})^{-1}M$ and $N_{k+1} = (F^{k+1})^{-1}N$, with the deformation gradient being $F^{k+1} = \partial X_{REF}/\partial X_{k+1}$.

Step iv: The counter k is incremented.

Step v: The infinite error norm is computed and, if it is less than TOL or the number of iterations is greater than $itemax$, the algorithm stops.

Step-5: Computer Simulation and Sensitivity Analysis

The pipeline (see in Fig. 1) has been implemented using a combination of the Matlab software (used for computing the geometrical reconstruction), the ABAQUS software (responsible for solving the FE problem), and an in-house C program for meshing. As described previously, the methodology is modular and the resulting FE model could be used to perform different computer simulations as for instance: eye inflation, surgical interventions and non-contact tonometry test among others.

A sensitivity analysis of the main parameters governing the numerical response of the in-silico model (displacement, U_{Num}) has been addressed in two key aspects: (i) the influence of introducing a random perturbation on the cornea's fiber orientation based on the human cornea's collagen dispersion reported in the literature;[19] (ii) the influence of 5 parameters governing the mechanical response of the cornea: intraocular pressure–IOP, central corneal thickness–CCT and material parameters–C_{10}, k_1, k_2.

The effect of the dispersion of the collagen fibers in humans reported by Meek et al.[19] is analyzed by introducing a random perturbation on the numerical fiber's pattern about the main orientations (nasal–temporal and superior–inferior). A healthy normal eye with three different levels of IOP (8, 12 and 30 mmHg) and fiber dispersion (0, 5 and 10 degrees), that comprises the reported range, has been considered, resulting in 9 additional computations.

In addition, a screening of the influence of the main parameters involved in the numerical simulation (IOP, CCT and material parameters) has been performed by means of a 2^k full factorial design[5,20] extending those reported previously,[10,11] that takes into account k different variables at 2 different levels (Low and High). Since it is a basic study, the parameter variation (see Table 2) was considered as follows: the IOP was considered to range on our extreme clinical values (8 and 30 mmHg) and the corneal material parameters were considered within a 50% of variation relative to the reference values for the conducted simulations. The geometry was based on a modification of a healthy eye (as used for analysis of the influence of the fiber dispersion) in which a constant thickening and thinning of the corneal thickness was applied to obtain different CCTs (this adaptation of the corneal thickness was performed by modifying the posterior corneal surface in order to preserve the anterior corneal curvature).

Hence, a full factorial analysis of 5 variables at 2 different levels was carried out, resulting in 32 additional simulations. Additionally, the study of the main effects of the parameters, the interaction among them and the analysis of variances (using a N-way ANOVA analysis) were derived from the full factorial analysis to

TABLE 2. Levels of parameter's variation (Low and High) involved in the 2^k factorial design (IOP: intraocular pressure; CCT: central corneal thickness; material parameters: C_{10}, k_1 and k_2). Reference parameters used for the conducted simulations are also included.

Case	IOP (mmHg)	CCT (μm)	C_{10} (MPa)	k_1 (MPa)	k_2 (–)
Reference	12	583	0.05	130.9	2490
Low	8	450	0.025	65.45	1245
High	30	680	0.075	196.35	3735

determine the most influential parameters on the numerical displacement.

Finally, to demonstrate the robustness and capabilities of the proposed methodology, a non-commercial non-contact tonometry test is simulated on a population of 130 eyes. Simulations based on the image-based geometry and simulations based on the zero-pressure geometry have been performed for a total of 260 finite element analysis. Statistical analyses were performed in Matlab R2012 v.8.0, and data are reported by their mean and standard deviation (mean $\pm$ SD), respectively. Statistical significance was tested with the two-sample Kolmogorov–Smirnov test, where a two-sided p-value of less than 0.05 determined significance.

RESULTS

Results obtained with the proposed pipeline for the patient-specific corneal modeling are presented in this section. First, in "Effect of the Zero-Pressure Configuration" section, the entire pipeline is demonstrated when studying the effect of accounting for the zero-pressure configuration on the simulation by testing the three sample cases used for checking the performance of the corneal reconstruction algorithm ("Step-2: Corneal Surface Reconstruction" section, Fig. 3). In "Sensitivity Analysis" section, results regarding the sensitivity analysis are presented and, finally, the study is further and automatically extended to a larger population of 130 patients considering both the zero-pressure configuration and the image-based configuration ("Effect of the Zero-Pressure Configuration: A Large Population Study" section).

Effect of the Zero-Pressure Configuration

To check the influence of the zero-pressure configuration on the numerical simulation of the eye mechanics, the general non-contact tonometry test has been simulated as described in the "Material and Methods" section. The maximum and the time evolution of the apical displacement have been computed for three different levels of IOP (10, 19, and 28 mmHg), for the three geometric models described in the previous section (see in Fig. 3). Hence, each geometry was subjected to the procedure shown in Fig. 1 for each IOP value.

Figure 7 shows the apical displacement of the healthy eye for the three different levels of IOP, obtained with the zero-pressure model and the image-based model. Incorporating the initial stress of the cornea results in a stiffer corneal response to the air-puff (lower apical displacement), as evidenced in Fig. 7b which shows that the initial pre-stress produces a shift in the maximum apical displacement vs. pressure curve. In addition, Fig. 7a shows that the effect of the initial stress is more noticeable as the pressure of the air-puff increases as demonstrated by the divergence in the apical displacement time course between the two models (image-based geometry and zero-pressure geometry), from the moment in which the deformation of the cornea becomes significant to the maximum difference when the air-puff reaches its maximum pressure ($t = 15$ ms). Note also that the divergence between the two curves initiates earlier for lower IOP values as shown in Fig 7a. This behavior shown in Fig. 7 is also observed in the KTC and post-LASIK geometries.

Table 3 shows the percentage of increase in the apical displacement due to the initial corneal pre-stress for different IOP and all geometries. The KTC model experiences the largest increment in apical displacement, whereas the Healthy model experiences the lowest increment in displacement. This result correlates well with the lower corneal pachymetry associated with the KTC and post-LASIK geometries.[2]

Sensitivity Analysis

Regarding the influence of the random perturbation of the collagen fibers orientation on the numerical displacement, the percentage difference in the corneal displacement (Δ_U^{apical}) among the models presenting random shift on the fibers and the original models with no dispersion is presented in the Table 4, showing that the maximum error does not exceed 0.03% in any combination. Hence, the influence of the fiber dispersion in the results is rather small.

The results of the 32 combinations for the 2^k full factorial analysis and the results of the N-way ANOVA analysis are presented in Tables 5 and 6 respectively. The first primary results came from locally comparing the 12 experiments determined by Cotter's method,[5] i.e., comparing the minimum reference level (all parameters set to the low level, $-$, see in Table 5) with respect to the other 5 levels with all parameters set to the low level ($-$) except for the parameter under analysis which is set to the high level ($+$) and, vice versa, comparing the maximum reference level (all parameters set to the high level, $+$, see in Table 5) with respect to the other 5 levels with all parameters set to the high level ($+$) except for the parameter under analysis which is set to the low level ($-$). On the one hand, in terms of a local relative percentage difference in displacement with respect to the maximum displacement (Test 1, $U_{Num} = 2.563714$), those that seem to be the most influential parameters, since they show the highest relative decrement on displacement, are the IOP (Test 2, -45.9%), the CCT (Test 3, -50.0%) and the k_1 (Test 9, -41.3%), whereas the least influential
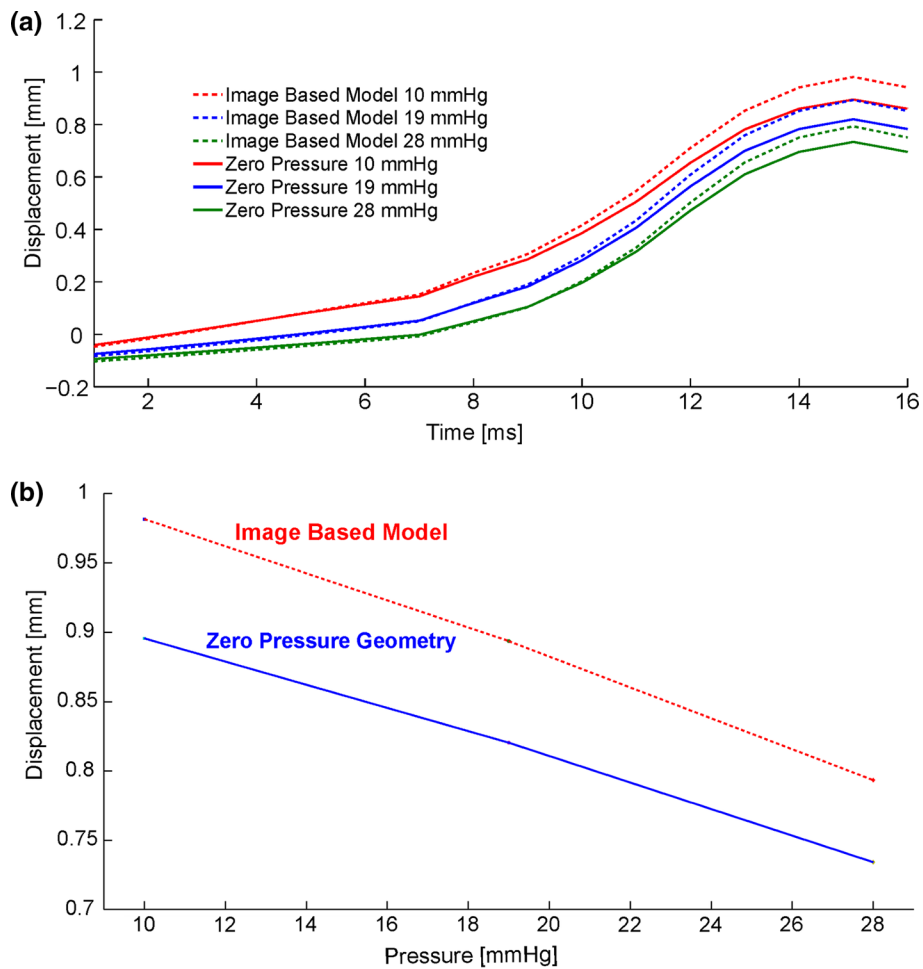
(a)

(b)

FIGURE 7. Effect of the initial stress in the healthy eye. (a) Evolution of the apical displacements for different IOP: (i) zero-pressure model (discontinuous lines), and (ii) image-based model (continuous line); (b) Maximum apical displacement for different IOP.

TABLE 3. Displacement difference between the image-based geometry (measured by the topographer) and the zero-pressure geometry (obtained with the free-stress algorithm) for the three different extreme geometries (Healthy, KTC and post-LASIK) and levels of IOP (10, 19 and 28 mmHg).

IOP (mmHg)	$\Delta_U^{apical} = 100 \cdot (U_{noZP}^{apical} - U_{ZP}^{apical})/U_{ZP}^{apical}$ (%)		
	Healthy	KTC	Post-LASIK
10	7.5	17.5	15.5
19	8.2	20.0	13.8
28	3.1	18.9	16.5

TABLE 4. Displacement difference between models with random shift on fibers dispersion (5, 10) and models with no-dispersion for three different levels of IOP (8, 12 and 30 mmHg).

IOP (mmHg)	$\Delta_U^{apical} = 100 \cdot (U_{5/10}^{apical} - U_0^{apical})/U_0^{apical}$ (%)		
	0-degrees	5-degrees	10-degrees
8	0	0.0006	0.0019
12	0	0.0011	0.0036
30	0	0.0076	0.0266

are C_{10} (Test 5, -9.9%) and k_2 (Test 17, -7.6%). On the other hand, in terms of a local relative percentage difference in displacement with respect to the minimum displacement (Test 32, $U_{Num} = 0.547892$), those that seem to be the most influential parameters, since they show the highest relative increment on displacement, are the IOP (Test 31, 21.0%), the CCT (Test 30, 76.9%) and the k_1 (Test 24, 32.3%), whereas the least influential are C_{10} (Test 28, 6.7%) and k_2 (Test 16, 0%).

A more complete analysis is achieved by observing the *p*-values and the *F*-statistic (*F*) of each Source (main effect of a parameter or interaction between different main parameters) presented in Table 6. According to these results, the IOP, CCT and k_1 are the most influential parameters on the numerical displacement (U_{Num}) since their *F*-statistics and their *p*-values are the highest, whereas C_{10} presents a significant but

TABLE 5. 2^k **full factorial design combinations ($2^5 = 32$) and the resulting objective variable** *y* **(Numerical Displacement of de Corneal Apex, U_{Num}) measured in millimetres.**

Exp.	IOP	CCT	C_{10}	k_1	k_2	$y - U_{Num}$ (mm)
Test 1	−	−	−	−	−	2.563714
Test 2	+	−	−	−	−	1.386425
Test 3	−	+	−	−	−	1.152660
Test 4	+	+	−	−	−	0.812387
Test 5	−	−	+	−	−	2.307931
Test 6	+	−	+	−	−	1.325756
Test 7	−	+	+	−	−	0.971684
Test 8	+	+	+	−	−	0.736133
Test 9	−	−	−	+	−	1.504956
Test 10	+	−	−	+	−	1.037734
Test 11	−	+	−	+	−	0.745937
Test 12	+	+	−	+	−	0.588232
Test 13	−	−	+	+	−	1.379099
Test 14	+	−	+	+	−	0.985989
Test 15	−	+	+	+	−	0.667031
Test 16	+	+	+	+	−	0.547892
Test 17	−	−	−	−	+	2.368668
Test 18	+	−	−	−	+	1.343527
Test 19	−	+	−	−	+	1.114085
Test 20	+	+	−	−	+	0.796277
Test 21	−	−	+	−	+	2.136569
Test 22	+	−	+	−	+	1.284817
Test 23	−	+	+	−	+	0.947469
Test 24	+	+	+	−	+	0.724942
Test 25	−	−	−	+	+	1.437088
Test 26	+	−	−	+	+	1.018412
Test 27	−	+	−	+	+	0.740186
Test 28	+	+	−	+	+	0.584746
Test 29	−	−	+	+	+	1.322432
Test 30	+	−	+	+	+	0.969044
Test 31	−	+	+	+	+	0.663006
Test 32	+	+	+	+	+	0.545347

TABLE 6. Analysis of variance (N-way ANOVA).

Source	Sum Sq.	d.o.f.	F	p-value
IOP	1.68125	1	226.29	0.0000
CCT	4.52565	1	609.13	0.0000
C10	0.08819	1	11.87	0.0033
k1	1.63620	1	220.22	0.0000
k2	0.01606	1	2.16	0.1609
IOP*CCT	0.50066	1	67.39	0.0000
IOP*C10	0.01922	1	2.59	0.1273
IOP*k1	0.27569	1	37.11	0.0000
IOP*k2	0.00526	1	0.71	0.4127
CCT*C10	0.00148	1	0.20	0.6610
CCT*k1	0.26089	1	35.12	0.0000
CCT*k2	0.00797	1	1.07	0.3156
C10*k1	0.00861	1	1.16	0.2976
C10*k2	0.00012	1	0.02	0.9017
k1*k2	0.00413	1	0.56	0.4665
Error	0.11887	16		
Total	9.15026	31		

Source source of variability, *Sum Sq.* the sum of squares due to each source, *d.o.f.* the degree of freedom of the *Source*; *F* the *F-statistic* which is the ratio of the mean squares; *p*-value the probability that the *F–statistic* can take a value larger than computed test-statistic value (p-value > 0.05 means non-significant effect or influence).

low influence and k_2 is non-significant (p-value = 0.1609). Furthermore, the IOP–CCT interaction, IOP–k_1 interaction, and CCT–k_1 interaction seem to play a non-negligible role in the numerical response (p-values = 0.0). In addition, by analyzing the percentage of influence of each parameter in terms of its deviation with respect to its average value[20] (Sum Sq. in Table 6), it can be highlighted that CCT, IOP, k_1, IOP–CCT and IOP–k_1 interactions represent more than the 95% of the influence on U_{Num}, whereas C_{10} represents less than 1% influence (see Pareto's diagram in Fig. 8a and pie chart in Fig. 8b).

The main effect of the present parameters on U_{Num} is further depicted in Fig. 8c, reinforcing the idea of the strong influence of CCT, IOP and k_1 on the numerical yield since they present a large range of variation and a pronounced inverse slope, i.e., the lower the level of the parameter, the higher the yield, whereas C_{10} presents a less pronounced slope and k_2 shows an almost constant response. Moreover, the interaction between the most influential parameters (CCT, IOP and k_1) is depicted in Fig. 8d, since there are no crossings or changes in their trends, a full inverse correlation is demonstrated for all the involved parameters: the highest level of the parameter will lead to the lowest level of the numerical displacement and vice versa.

Effect of the Zero-Pressure Configuration: A Large Population Study

To gain a better understanding on the effect of the zero-pressure configuration, and to demonstrate the potential of the proposed methodology, a population of 130 patients (53 healthy, 63 KTC and 14 post-LASIK eyes) was analyzed. Topographical data were acquired with a Pentacam topographer and the patient's IOP with a Goldman's Applanation Tonometer (C.S.O. Srl). In order to validate the methodology, results from the numerical simulation were compared with clinical results obtained with a CorVis ST system reported in the literature (60 Healthy and KTC eyes,[28] and 52 post-LASIK eyes 30 days after surgery[12]). In addition to the apical displacement, the minimum principal stress, σ_{min}^{Apx}, and minimum principal stretch, λ_{min}^{Apx}, at the apex of the anterior surface have been taken into account.

Table 7 shows the mean and standard deviation of the three biomarkers obtained for the three populations with the image-based model and the zero-pressure model. Clinical results for the maximum apical displacement from the literature are also shown for completeness. Although results of the apical displacement are within the range obtained in clinical studies, the apical displacements obtained with the zero-pres-

FIGURE 8. Sensitivity analysis. (a) The cumulative percentage of contribution of the parameters on the numerical displacement (%). The most important parameters that describe the numerical response with a 95% of confidence are the central corneal thickness (CCT–50%), the intraocular pressure (IOP–19%) and the material parameter associated with the fiber strength (k_1–18%). In addition, the interactions among IOP, CCT and k_1 comprise a 10% of the influence on the numerical response; (b) The total contribution of the analyzed parameters to the numerical response (C_{10} contributes less than a 1% and k_2 presents non-significative influence); (c) The main effects of the analyzed parameters on the numerical displacement (CCT, IOP and k_1) show a highest inverse influence (low parameter's level results in the highest displacement and vice versa) whereas C_{10} and k_2 presents almost a constant influence; (d) The main interaction effects among the most influential parameters (CCT, IOP and k_1) show a high inverse correlation between all parameters, resulting on the highest displacement when the lowest effects are considered, whereas the lowest displacement is achieved when the highest effects are considered.

sure model underestimate the clinical results, whereas those obtained with the image-based model overestimate the maximum apical displacement. A two sample Kolmogorov–Smirnov test on the apical displacement have shown no significant differences (p-value > 0.05) between post-LASIK–KTC, but have shown significant differences between KTC–Healthy and post-LASIK–Healthy for both, the image-based and the zero-pressure models, in agreement with clinical results.[12,28] The same results were found for the stress and stretch biomarkers. However, when comparing the results obtained with the zero-pressure model and the image-based model for the same biomarker, significant differences in all three biomarkers were only found for the Healthy eye, whereas for the KTC and post-LASIK eye, significant differences were only found for the maximum apical displacement.

The effect of the zero-pressure configuration is better appreciated in Fig. 9 where the percentage difference between the biomarkers computed with the image-based model and the zero-pressure model during the air-puff are depicted (the zero-pressure model is taken as reference). A larger dispersion is present in all biomarkers for the KTC cases in comparison with the Healthy and the post-LASIK populations. Furthermore, the stiffer response of the cornea due to the incorporation of the zero-pressure configuration is also demonstrated, as the average apical displacement is always smaller for the image-based model than for the zero-pressure model (positive percentage) at all instants during the air-puff. However, this effect becomes more relevant as the pressure of the air-puff increases (maximum at 15 ms in the figure), coinciding with the maximum deformation of the cornea, and when the nonlinear response of the material becomes noticeable.
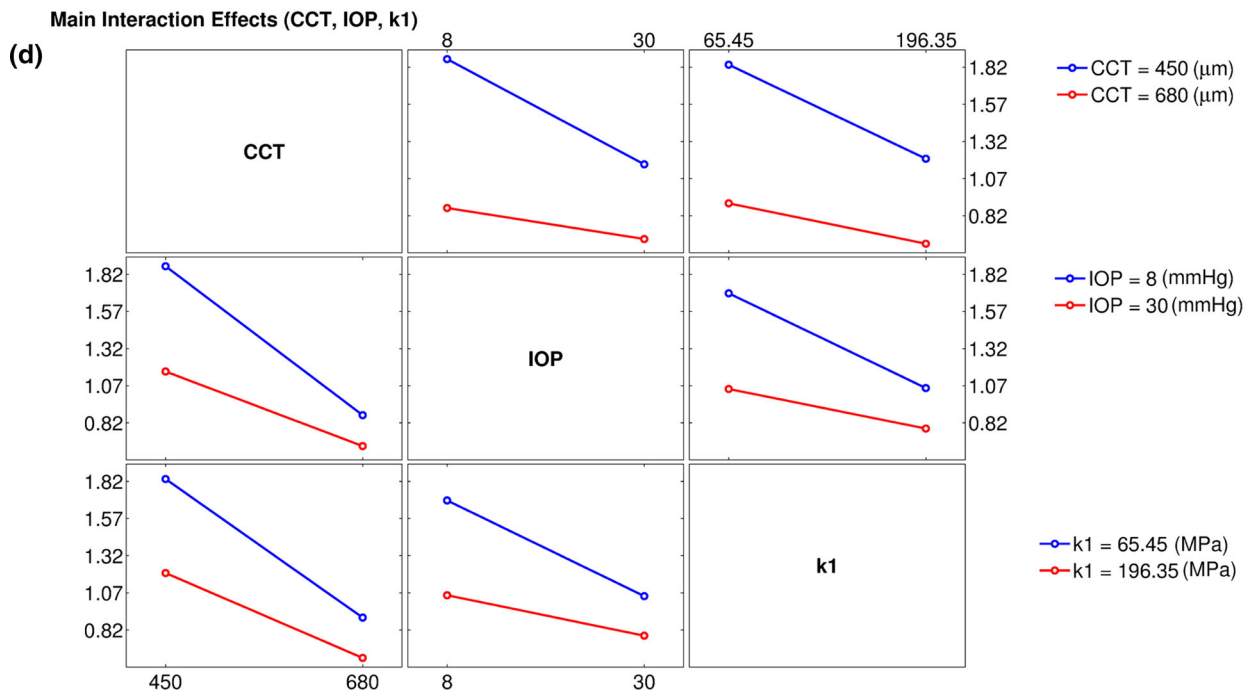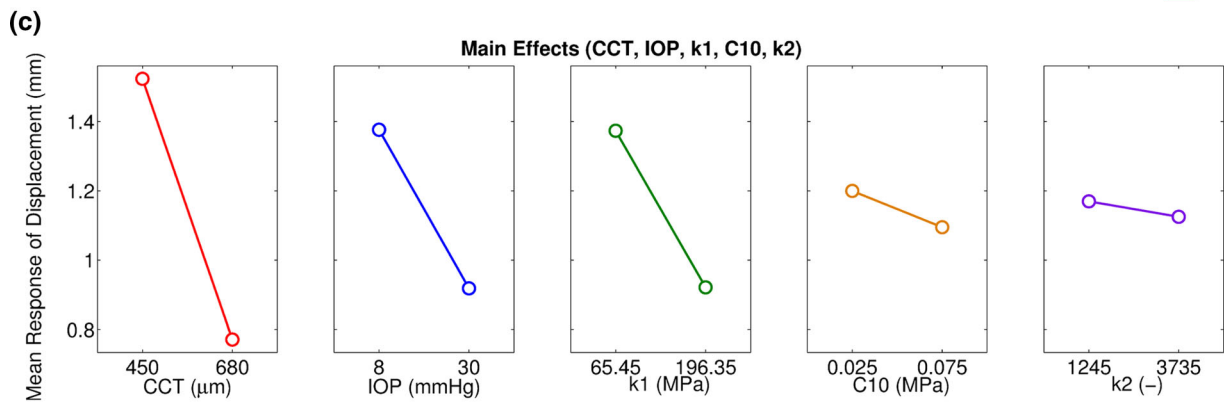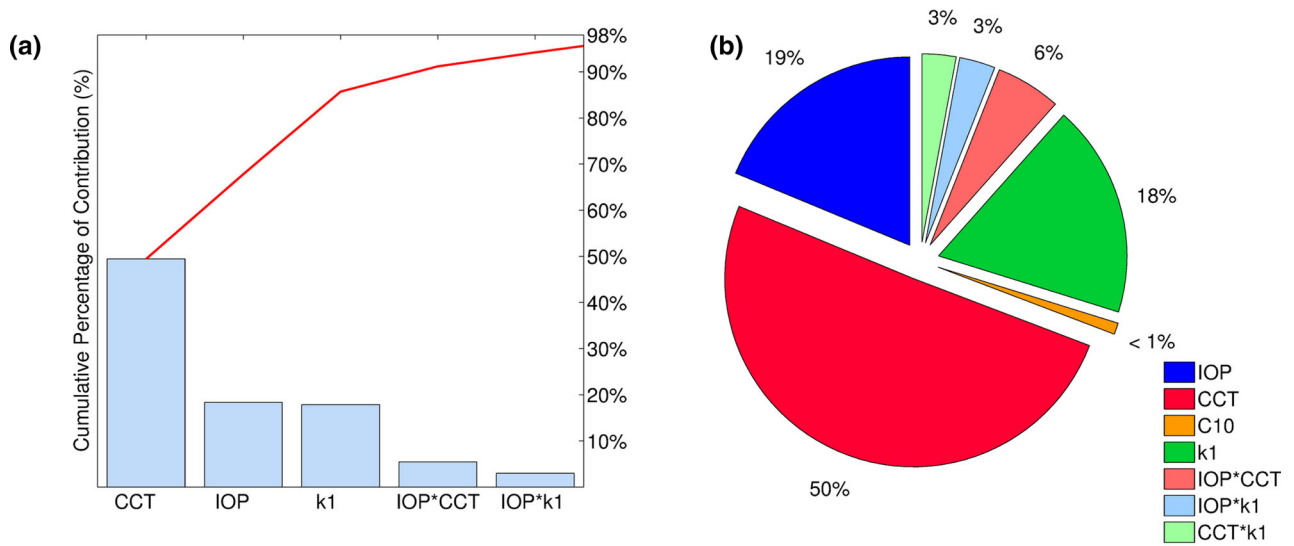
TABLE 7. Statistics of numerical results: (i) Maximum Apical Displacement, *U* (mm), (ii) Minimum in-plane principal stress at the apex of the anterior corneal surface, σ_{min}^{Apx} (MPa), and (iii) Minimum in-plane principal stretch at the apex of the anterior corneal surface, λ_{min}^{Apx} [–], computed with the image-based and zero-pressure models. Clinical results from the literature are also included[12,28] (mean ± standard deviation).

| Results	Healthy	KTC	Post-LASIK
Apex Pac. (μm)	553.8 ± 36.2	472.1 ± 69.3	501.1 ± 53.9
IOP$_{GAT}$ (mmHg)	13.5 ± 2.2	12.3 ± 2.6	11.6 ± 1.6
Image-based model			
U (mm)	1.04 ± 0.14	1.20 ± 0.19	1.15 ± 0.11
σ_{min}^{Apx} (MPa)	−0.476 ± 0.075	−0.624 ± 0.156	−0.556 ± 0.078
λ_{min}^{Apx} [–]	0.959 ± 0.002	0.955 ± 0.003	0.957 ± 0.002
Zero-pressure model			
U (mm)	0.93 ± 0.11	1.07 ± 0.17	1.03 ± 0.10
σ_{min}^{Apx} (MPa)	−0.440 ± 0.071	−0.573 ± 0.138	−0.520 ± 0.077
λ_{min}^{Apx} [–]	0.960 ± 0.002	0.956 ± 0.003	0.958 ± 0.002
Clinical Results			
Apex Pac. (μm)	520.0 ± 25.0	475.0 ± 38.0	524.0 ± 63.2
IOP$_{CorVis}$ (mmHg)	14.4 ± 2.5	14.4 ± 2.2	14.2 ± 4.2
U (mm)	1.04 ± 0.10	1.13 ± 0.12	1.08 ± 0.14
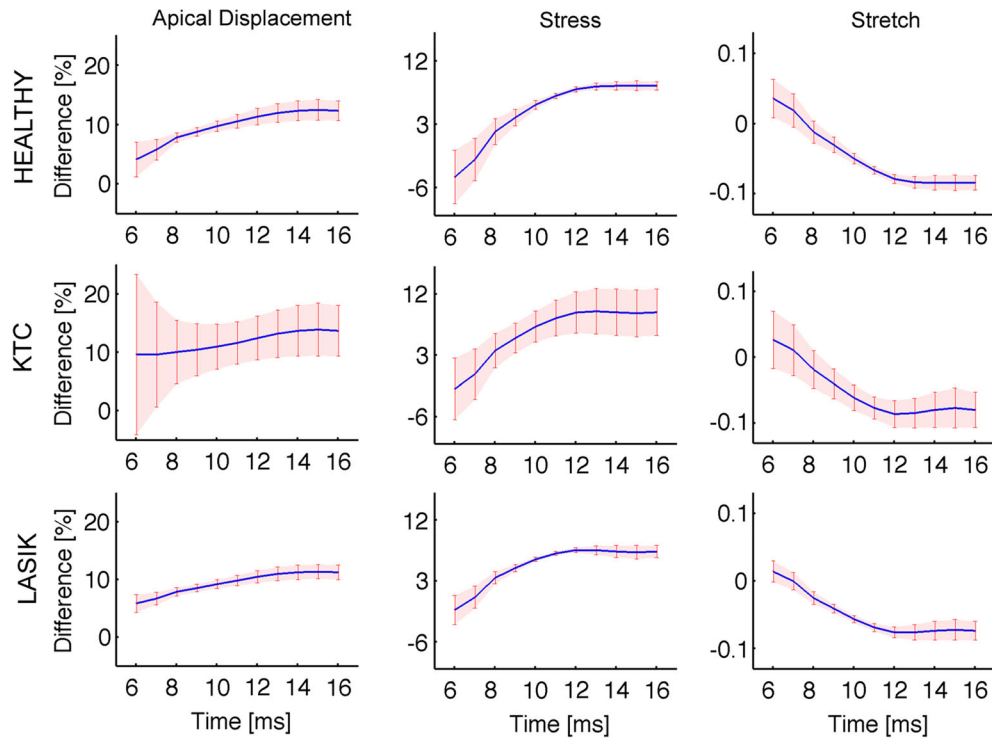
FIGURE 9. Percentage difference of the biomarkers between the image-based model and the zero-pressure model (blue line is the average response and and red bars the dispersion) at each instant during the air-puff. First row corresponds to the Healthy population, second row to the KTC population, and third row the post-LASIK population. Left column corresponds to the apical displacement, *U*; Middle column to the minimum in-plane principal stress at the apex of the anterior surface of the cornea, σ_{min}^{Apx}; Right column to the minimum in-plane principal stretch at the apex of the anterior surface of the cornea, λ_{min}^{Apx}.

Table 8 summarizes the percentage difference in the biomarkers for the high concavity time ($t = 15$ ms). It is remarkable that the average percentage difference for each biomarker is very similar for the three populations, with a significant larger dispersion in the case of KTC eyes.

DISCUSSION

A novel automatized methodology to generate an FE model by incorporating the patient-specific corneal topographic data and which is amenable for different numerical simulations is proposed. Contrary to previ-

TABLE 8. Difference in biomarkers (%) at the high concavity time ($t = 15$ ms) for the three populations, taking the zero-pressure model as reference. Results given as mean ± standard deviation.

Biomarker	Healthy	KTC	Post-LASIK
U	12.162 ± 2.217	13.043 ± 5.039	11.339 ± 1.253
σ_{min}^{Apx}	8.358 ± 0.730	8.873 ± 3.442	7.194 ± 1.011
λ_{min}^{Apx}	-0.084 ± 0.012	-0.075 ± 0.029	-0.072 ± 0.015

ous methodologies,[29,32] the proposed approach does not approximate the topographical data where it is known, increasing the fidelity of the reconstructed patient model (see Fig. 2c). The implementation of the proposed pipeline using Matlab, ABAQUS and an in-house C-code takes about 90 min to complete on a single patient: approximately 30 min in the model construction phase, and about 60 min for the finite element simulation (non including the zero-pressure algorithm) in a conventional PC with 8 core processor and 8 GB RAM. A more optimized implementation of the pipeline could substantially reduce these times, making the proposed methodology feasible for clinical use as an aided-diagnosis tool.

Furthermore, the mesh convergence analysis has demonstrated the importance of the finite element mesh used in the computations, particularly when modeling a non-contact tonometry test for which the bending behavior of the cornea must be accurately captured.[16,35] Therefore, linear (four nodes tetrahedra) or trilinear elements (eight nodes hexahedra) must be used carefully since these elements do not capture the bending behavior properly. A sufficiently large number of elements through the thickness must be used in order to achieve accurate results (see Fig. 5b). In this regard, the best trade-off between numerical accuracy and computation time when modeling a non-contact tonometry test was obtained with 20-node quadratic elements and 5 elements through the corneal thickness (186,828 D.O.F.).

Results derived from the sensitivity analysis can be assumed to represent the general numerical behavior of the entire population, despite only using a single healthy model, since the analyzed range of physiological parameters (IOP, CCT) covers the most extreme values of the corneal features belonging to the different population groups (the IOP ranges from 8 to 30 mmHg (glaucoma) and the CCT ranges from 450 microns (KTC) to 680 microns beyond the healthy range), whereas the material parameters were varied 50% with respect to the material selected for the conducted simulations (C_{10} related to the ground matrix, k_1 related to the fiber strength over the stretch direction and k_2 which controls the fiber behavior under very large deformations). The CCT, whose contribution in the

response perturbation is 50%, the IOP (19%) and the k_1 (18%) have been found to be the most influential parameters in the numerical displacement, whereas the remaining parameters (C_{10} and k_2) seem to have a negligible contribution on the response variation (see Table 6; Fig. 8). Furthermore, these results are supported in physical terms since the thickness (CCT) follows an inverse cubic relationship with the displacement when a shell is subjected to bending,[2] IOP represents a constant opposite force to external forces which greatly modifies the deformation amplitude of the corneal apex, and k_1 represents the fiber's resistance to stretching: the higher the stretching (deformation), the higher the contribution of the fibers. The ground matrix term (C_{10}) does not seem to play a major role in the numerical problem due to a two-fold reason: its contribution to the global stiffness is quite small and the global response of the cornea is governed by bending (see Fig. 10). Finally, the k_2 would play a major role should the cornea reach higher intraocular pressures, however, the material response is dominated by the k_1 term in the physiological IOP range. Hence, the results of the sensitivity analysis along with the ANOVA analysis show a full inverse correlation among all the parameters and the numerical displacement and, in addition, further demonstrate that the apex displacement obeys an interplay among the geometry, the mechanical behavior of the cornea (material properties) and the intraocular pressure as has been previously reported.[2]

The methodology has also been applied to evaluate, in a population of 130 patients (53 healthy eyes, 63 KTC eyes and 14 post-LASIK), the effect of the zero-pressure on the results of a general non-commercial non-contact tonometry simulation test. Numerical results were compared to reported clinical results obtained with a CorVis ST in order to validate the process, showing a good agreement between the numerical global response and the clinical tests. Additionally, our numerical results have been found to be in the same range as the numerical results reported by Kling et al.[16] However, Kling et al. have used numerical models of porcine and human corneas that accounted for different boundary conditions and a material model which included a viscoelastic contribution. It is important to note that our simulation did not pretend to model a particular commercial device, but only to replicate a typical evaluation test. Hence, the main characteristics of the test such as the peak pressure of the air-puff, or the location and duration of the air pulse, were set in order to emulate a general non-contact tonometer. In addition, some assumptions were made regarding the air pressure over the cornea. Even though the pressure has been assumed to vary in time and space (see Fig. 5a), shear effects on the cor-

neal surface due to the air-puff has been neglected. Our results also indicate that the initial pre-stress of the cornea due to the IOP stiffens the corneal response, leading to significant differences in the apical displacement obtained with the zero-pressure model and the image-based model. Furthermore, results for the KTC population showed a considerable larger dispersion as compared to the Healthy and the post-LASIK population, which correlates with the larger dispersion present in the pachymetry data for the KTC eyes.

This can also be related to the important effect of the corneal thickness on the corneal response when subjected to the action of an air-puff. In more detail, when subjected to an air-puff, the cornea passes from a pure tensile membrane state of stress due to the IOP, to a bending state of stress where the anterior surface experiences contraction while the posterior surface is in traction (see Fig. 10). Thus, the previous work presented in Ariza-Gracia *et al.*[2] helps to explain the significant sensitivity of the results to changes in corneal pachymetry, this being subsequently demonstrated in the sensitivity analysis, since, as aforementioned, the bending stiffness follows an inverse cubic relationship with the corneal thickness.

In this line of results, the study conducted on Healthy, KTC and post-LASIK eyes gave values for the apical displacements within the range of clinical results[12,15,28,34] even though all models have used the same corneal material. Therefore, this fact along with the present sensitivity analysis may suggest that the geometrical corneal features could be more important than the corneal tissue considerations when only the maximum bending apex displacement is studied.

Finally, although the proposed pull-back algorithm used to find the free-stress configuration of the eye is similar to other approaches previously proposed in the literature,[8,23,29] the present methodology has the advantage of being the first to incorporate a consistent mapping of the collagen fibers onto the current zero-pressure configuration of the eye. In addition, the proposed algorithm found the zero-pressure geometry in less than 10 iterations with a tolerated relative error of less than 0.2 microns (less than a 0.05% of the corneal thickness). Apart from the stiffening in the corneal response, our results also indicate that the proposed algorithm preserves the tissue volume globally, i.e., the zero-pressure and image-based geometries had the same volume (volume change less than 0.001%) and, moreover, the volume is also preserved locally with a maximum volume change of less than 0.3%. This is particularly important for three-dimensional solid simulations, since the cornea, the limbus and the sclera are considered incompressible materials. This feature of the algorithm is a consequence of using a quasi-incompressible material description for the different tissues, in addition to the nearly polar symmetry of eye that causes almost a radial deformation under the the action of the IOP.

Last but not least, the study presents a number of limitations. The same material anisotropic properties for the cornea and the limbus for all patients have been considered, including neither the patient-specific material parameters nor the patient-specific collagen fibers pattern. However, to date, the only available human data in the literature is limited to pressure-apical rise curves on a small number of patients, pro-
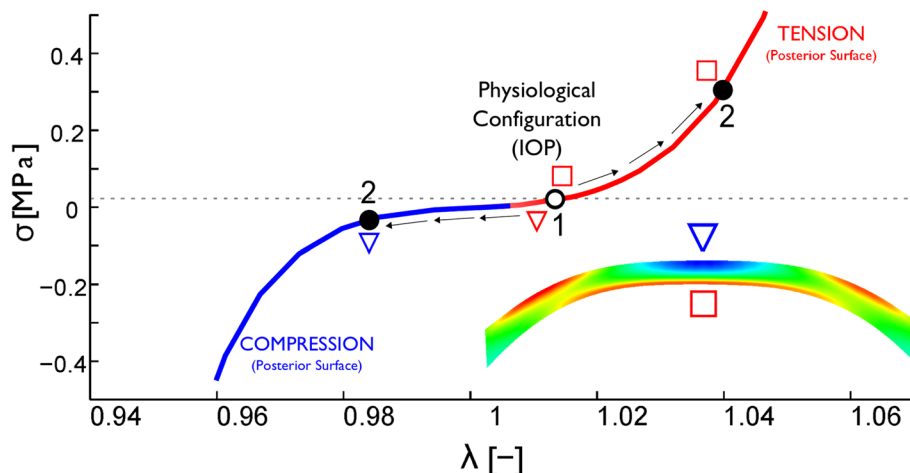

FIGURE 10. Apex stress-stretch ($\sigma - \lambda$) behavior for the Healthy eye with an IOP of 19 mmHg. At the beginning of the simulation (1. Physiological configuration after zero-pressure algorithm), both surfaces start at $\lambda > 1$ (physiologic pre-stress) but, when an air-puff is applied onto the cornea and it bends, the anterior surface (inverted triangle at point 2) works in compression and shortens its length (stretch less than 1 (*blue*)), whereas the posterior surface (square at point 2) works in tension and the local corneal tissue lengthens (stretch greater than 1 (*red*)).

viding only a range of mechanical response. For this reason, we have decided to use a set of parameters that fit a particular curve within the reported range as shown in Fig. 4b, although accounting for the variability in the mechanical properties will certainly affect the variability in the biomarkers (Table 7), as further demonstrated in the sensitivity analysis (see Table 6; Fig. 8). Therefore, the main conclusions regarding the influence of the zero-pressure configuration on the simulation results will not be affected. Moreover, although a fixed general pattern of collagen fibers is used, the random perturbation of the collagen fibers following the results of Meek et al.,[19] does not quantitatively affect the numerical displacement (a maximum of a 0.03% of variation, see Table 4). Finally, the material model could be improved by considering the viscoelastic behavior.[16]

In conclusion, a novel in-silico methodology to generate an FE model that incorporates the patient-specific corneal geometry has been proposed. The pipeline allows in-silico tests to carry out a sensitivity analysis of the mechanical properties of the corneal tissue, the IOP, and the geometry of the cornea on the corneal deformation of patient-specific geometric eye models. This allows improved understanding of the eye biomechanics, as well as helping to plan surgeries, i.e., LASIK surgeries, or to interpret the results of new diagnosis tools, as in the case of noncontact tonometers. The proposed methodology could also be applied for performing inverse FE analysis on a patient-specific corneal model in order to identify the mechanical parameters on the patient's cornea.

REFERENCES

[1]Alastrué, V., Calvo, B, Peña, E, and Doblaré, M. Biomechanical odeling of refractive corneal surgery. *J. Biomech. Eng.*, 128(1):150–160, 2006.

[2]Ariza-Gracia, M. Á., Zurita, J. F., Piñero, D. P., Rodriguez-Matas, J. F., and Calvo, B. coupled biomechanical response of the cornea assessed by non–contact tonometry.

a simulation study. *PLoS One* 10(3):e0121486. doi 10.1371/journal.pone.0121486.

[3]Bourges, J. L., Alfonsi, N., Laliberté, J. F., Chagnon, M., Renard, G., Legeais, J. M., and Brunette I. Average 3-dimensional models for the comparison of orbscan ii and pentacam pachymetry maps in normal corneas. *Ophthalmology*, 116(11):2064–2071, 2009.

[4]Bryant, M. R. and McDonnell, P.J. Constitutive laws for biomechanical modeling of refractive surgery. *J. Biomech. Eng.*, 118(4):473–481, 1996.

[5]Cotter, S. C. A screening design for factorial experiments with interactions.*Biometrika* 66(2):317–320, 1979.

[6]Coudrillier, B., Pijanka, J. K., Jefferys, J., Sorensen, T., Quigley, H.A., Boote, C., and Nguyen, T. D. Effects of age and diabetes on scleral dtiffness. *J. Biomech. Eng.*, 137:061004, 2015. doi:10.1115/1.4029986.

[7]Eilaghi, A., Flanagan, J. G., Tertinegg, I., Simmons, C. A., Brodland, G. W., Ethier C.R. and Biaxial. Mechanical testing of human sclera. *J. Biomech.*, 43(9):1696–1701, 2010.

[8]Elsheikh, A., Whitford, C., Hamarashid, R., Kassem, W., Joda, A., and Büchler, P. Stress free configuration of the human eye. *Med. Eng. Phys.*, 35(2):211–216, 2013.

[9]Gasser, T. C., Ogden, R. W., and Holzapfel, G. A. Hyperelastic modeling of arterial layers with distributed collagen fiber orientations. *J. R. Soc. Interface*, 3(6):15–35, 2006.

[10]Girard, M. J. A., Downs, J. C., Bottlang, M., Burgoyne, C. F., and Suh, J.-K. F. Peripapillary and posterior scleral mechanics-part II: experimental and inverse finite element characterization. *J. Biomech. Eng.*, 131(5):051012, 2009.

[11]Girard, M. J. A., Downs, J. C., Bottlang, M., Burgoyne, C. F., and Suh J.-K. F. Peripapillary and posterior scleral mechanics-part I: development of an anisotropic hyperelastic constitutive model.*J. Biomech. Eng.* 131(5):051011, 2009.

[12]Hassan, Z., Modis, L., Szalai, E., Berta, A., and Nemeth, G. examination of ocular biomechanics with a new Scheimpflug technology after corneal refractive surgery. *Cont. Lens Anterior Eye*, 37:337–341, 2014.

[13]Holzapfel, G. A., Gasser, T. C., and Ogden R. W. A new constitutive framework for arterial wall mechanics and a comparative study of material models. *J. Elast. Phys. Sci. Solids*, 61(1–3):1–48, 2000.

[14]Hong, J., Xu, J., Wei, A., Deng, S. X., Cui, X., Yu, X., and Sun X. A new tonometer-the CorVis ST tonometer: clinical comparison with noncontact and goldmann applanation tonometers. *Invest. Ophthalmol. Vis. Sci.*, 54(1):659–665, 2013.

[15]Huseynova, T., Waring, G.O., Roberts, C., Krueger, R. R., and Tomita M. Corneal biomechanics as a function of intraocular pressure and pachymetry by dynamic infrared signal and Scheimpflug imaging analysis in normal eyes. *Am. J. Ophthalmol.*, 157(4):885–893, 2014.

[16]Kling, S. and Marcos, S. Contributing factors to corneal deformation in air puff measurements. *Invest. Ophthalmol. Vis. Sci.*, 54(7):5078–5085, 2013.

[17]Kling, S., Bekesi, N., Dorronsoro, C., Pascual, D., and Marcos, S. Contributing factors to corneal deformation in air puff measurements. *PLoS One*, 9(8):e104904, 2014.

[18]Lanchares, E., Calvo, B., Cristóbal, J. A., and Doblaré, M. Finite element simulation of arcuates for astigmatism vorrection. *J. Biomech.*, 41(4):797–805, 2008.

[19]Meek, K. M. and Boote, C. The use of X-ray scattering techniques to quantify the orientation and distribution of collagen in the corneal stroma. *Prog. Retin Eye Res.* 28(5):369–392, 2009.

[20]Montgomery D. C. *Design and Analysis of Experiments* New York: Wiley, 5th edition, 1997. ISBN 0-471-31649−0.

[21]Newton, R. H. and Meek, K. M. The integration of the corneal and limbal fibrils in the human eye. *Biophys. J.*, 75(5):2508–2512, 1998.

[22]Ogbuehi, K. C. and Osuagwu, U. L. Corneal biomechanical properties: precision and influence on tonometry. *Cont. Lens Anterior Eye*, 37(3):124–131, 2014.

[23]Pandolfi, A. and Manganiello, F. A model for the human cornea: constitutive formulation and numerical analysis. *Biomech. Model. Mechanobiol.*, 5(4):237–246, 2006.

[24]Pandolfi, A. and Holzapfel, G. A. Three-dimensional modeling and computational analysis of the human cornea considering distributed collagen fibril orientations. *J. Biomech. Eng.*, 130(6):061006, 2008.

[25]Pinsky, P. M, van der Heide, D., and Chernyak, D. Computational modeling of mechanical anisotropy in the cornea and sclera. *J. Cataract. Refract. Surg.*, 31(1):136–145, 2005.

[26]Rabinowitz, Y. S. Keratoconus. *Surv. Ophthalmol.*, 42(4):297–319, 1998.

[27]Riveros, F., Chandra, S., Finol, E. A., Gasser, T. G., and Rodriguez, J. F. Pull-back algorithm to determine the unloaded vascular geometry in anisotropic hyperelastic aaa passive mechanics. *Ann. Biomed. Eng.*, 41(4):694–708, 2013.

[28]Roberts C. A journey through the biomechanics of the cornea. In *Conference ESOIRS*. The Ohio State University: Ohio, 2012.

[29]Roy, A. S. and Dupps, W. J. Patient-specific modeling of corneal refractive surgery outcomes and inverse estimation of elastic property changes. *J. Biomech. Eng.*, 133(1): 011002, 2011.

[30]Ruiseñor Vázquez, P. R., Galletti, J. D., Minguez, N., Delrivo, M., Fuentes Bonthoux, F., Pförtner, T., and Galletti, J. G. Pentacam Scheimpflug tomography findings in topographically normal patients and subclinical keratoconus cases. *Am. J. Ophthalmol.*, 158(1):32–40.e2, 2014.

[31]Runger, G.C. and Montgomery, D. C. Applied Statistics and Probability for Engineers, Vol.1. New York: Wiley, 2nd edn, 1999.

[32]Studer, H. P., Riedwyl, H., Amstutz, C. A., Hanson, J. V. M., and Büchler P. Patient-specific finite-element simulation of the human cornea: a clinical validation study on cataract surgery. *J. Biomech.*, 46(4):751–758, 2013.

[33]Thompson, J. F., Soni, B. K., and Weatherill, H. P. Handbook of Grid Generation. Boca Raton: CRC Press, 1998.

[34]Valbon, B. F., Ambrósio, R., Fontes, B. M, and Alves, M. R. Effects of age on corneal deformation by non-contact tonometry integrated with an ultra-high-speed (UHS) Scheimpflug camera. *Arq. Bras. Oftalmol.*, 76 (4):229–232, 2013.

[35]Whitford, C., Studer, H. P., Boote, C., Meek, K. M., and Elsheikh, A. Biomechanical model of the human cornea: considering shear stiffness and regional variation of collagen anisotropy and density. *J. Mech. Behav. Biomed. Mater.*, 42:76–87, 2015.